Fluid-Mechanical Interaction Simulation and Coupling Analysis for Deep Mining of Subsea Resources

Qifeng Guo[1, 2*], Qiannan Chen[1, 2], Shengjun Miao[1, 2], Xun Xi[1, 2], Zhaocai Zhang[1, 2]

[1] School of Civil and Environmental Engineering, University of Science and Technology Beijing, Beijing 100083, China
[2] Key Laboratory of High-Efficient Mining and Safety of Metal Mines (Ministry of Education of China), University of Science and Technology Beijing, Beijing 100083, China
**Corresponding author, E-mail: qifeng_024@163.com*

Abstract
Accounted for 71% of the earth surface, the ocean is rich in mineral resources. With the decreasing of mineral resources on land, subsea resources exploitation becomes the further development direction. Mineral mining in subsea bedrock is always in condition of rich water and high in-situ stress, and their distributions and fluid-mechanical interactions are significant factors affecting the safety of subsea mining. Based on deep mining in the costal mine of Sanshandao Gold Mine, series surveys and measurements on water and stress were carried out: investigated the aquifers in deep mine, measured the in-situ stress, analyzed the joint distribution, researched the of rock mass permeability, and built coupled fluid-mechanical numerical model to simulate the deep mining process. Above researches achieved the in-situ stress distribution law, permeability of rock masses in deep mine, the space-time evolutions of displacement and stress during the mining process and also the space-time distribution of potential hazards.
Key words: NUMERICAL SIMULATION, FLUID-MECHANICAL COUPLING ANALYSIS, SUBSEA RESOURCES, DEEP MINING, IN-SITU STRESS

1. Introduction

Accounted for 71% of the earth surface, the ocean is rich in mineral resources. Subsea resources include mineral deposits contained in shallow sediment and seafloor rock. Now the submarine oil and natural gas account for more than 90% among the developed values of subsea resources. With the decrease of mineral resources on land, many mines have entered into deep mining [1,2] and submarine mining[3,4] in order to get more resource. In Japan, the submarine coal mining has reached 30% of the total production, which means that the submarine mining is becoming the future trends in mineral development.

Subsea bedrock mineral mining is always in condition of rich water and high in-situ stress, and their distributions and fluid-mechanical interactions are significant factors affecting the safety of subsea deep mining, so during the mining process we have to consider the ground water, joints and in-situ stress distribution. Scholars have got many achievements mainly focused on theoretical model, experimental analysis and numerical simulation. Such as Qiping Wang[5] and Meifeng Cai[6], they

used numerical simulation to take out fluid-mechanical coupling analysis on the foundation and open pit slope based on the theoretical model and experimental analysis research, which proved the necessary and applicability of numerical simulation and fluid-mechanical coupling analysis in engineering problems.

In this paper, on the background of deep mining in the costal mine of Sanshandao, series surveys and measurements on water and stress were carried out: investigated the aquifers in deep mine, measured the in-situ stress, analyzed the joint distribution law, researched the of rock mass permeability, and built coupled fluid-mechanical numerical model to simulate the deep mining process. These researches achieved the in-situ stress distribution law, permeability of rock masses in deep mine, the space-time evolutions of displacement and stress during the mining process and also the space-time distribution of potential hazards.

2. Underground water and in-situ stress investigation

2.1 Underground water distribution

Sanshandao Gold Mine's aquifers are mainly water zones in rock fissures. As the ore-controlling structure F1 has water-resisting property, so the water zones influencing the mining process can be divided into F3 water zone, F1 hanging side water zone and F1 heading side water zone, according to their spatial position compared to F1.

F1 heading side water zone has direct influence on the deep mining process and construction engineering. On the difference of structural develop feature and groundwater recharge condition, F1 heading side water zone can be divided into rich water zones and containing water zones. The rich water zones have strong hydraulic conductivity in north-west direction with units-inflow of drill hole is 1-2 $L\cdot(s\cdot m)^{-1}$ and the maximum water emission 194 $m^3\cdot h^{-1}$. The containing water zones' hydraulic conductivity is weak, so the units-inflow of drill hole is 0.224 $L\cdot(s\cdot m)^{-1}$, and the maximum water emission is only 50 $m^3\cdot h^{-1}$.

Electrical measuring method is used to achieve the storage and distribution of underground water. The tests were carried out in the -510m level, and the tests results can be described in fig.1. There are many areas with resistivity below 100Ω·m. In vertical direction, the low resistivity areas are in -530m to -545m, and in horizontal direction, low resistivity areas lie in 90m、130m、180m、230m、300m、350m and 380m along the measuring line.

2.2 In-situ stress state

The in-situ stress state[7] can provide basis for optimum design of the mine in following aspects: overall layout of the mining engineering, selection of the optimal shape of underground roadways and stopes, selection of most suitable mining method and steps, design of reliable support and reinforcement of mining structures, prediction of rock burst, mining seismicity and other dynamic disasters. In-situ stress measurement were carried out at 13 points in Sanshandao Gold Mine, the results were shown in table 1 and the linear regression of principal stresses with depth can be drawn as figure 3.

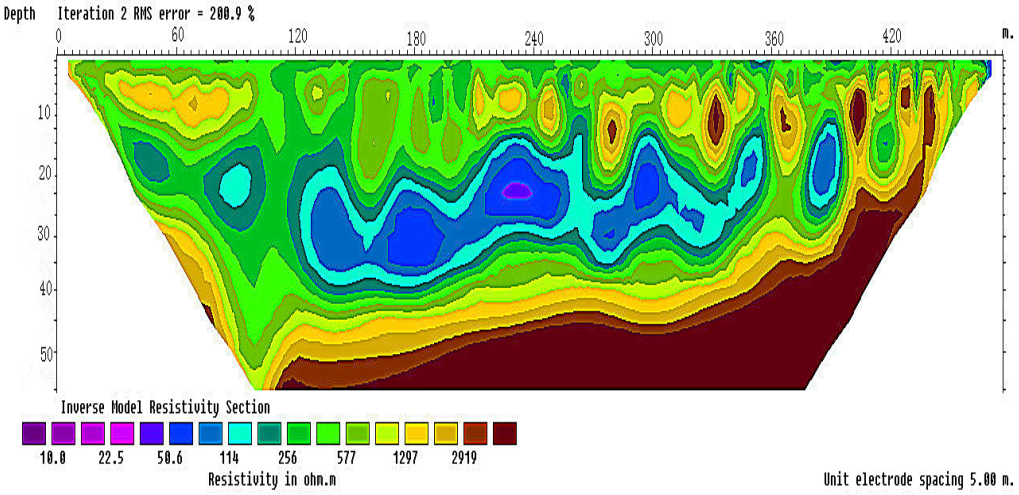

Figure 1. Geophysical inversion image

Table 1. Measuring results of *in-situ* stress state

Monitor	σ_1	σ_2	σ_3

depth / m		Magnitude / MPa	Bearing / (°)	Dip / (°)	Magnitude / MPa	Bearing / (°)	Dip / (°)	Magnitude / MPa	Bearing / (°)	Dip / (°)
1	-510	24.55	129	4	16.35	-138	2	14.49	133	-85
2	-510	24.64	-111	3	15.68	155	82	15.02	161	-10
3	-645	29.57	112	-3	19.56	-177	-80	15.48	-156	-9
4	-600	28.88	103	1	16.54	10	76	14.77	13	-8
5	-600	30.17	110	-16	18.83	24	-11	16.94	236	-70
6	-690	31.50	-80	2	19.08	230	-79	17.54	10	-10
7	-690	29.77	-83	4	20.84	-8	-74	19.63	8	15
8	-750	33.22	119	-10	19.93	-89	-82	17.10	208	-8
9	-555	25.71	-45	-13	14.00	14	73	13.00	50	-20
10	-75	6.01	288.5	-6.3	3.81	198.0	-4.9	2.56	250.4	82.0
11	-420	19.27	284.1	-21.3	11.05	18.5	-11.1	10.88	134.4	-65.7
12	-420	19.39	120.4	-14.9	10.92	169.2	68.1	9.44	34.7	15.8
13	-150	7.73	280.9	-5.2	5.48	9.4	16.6	4.50	27.7	72.5

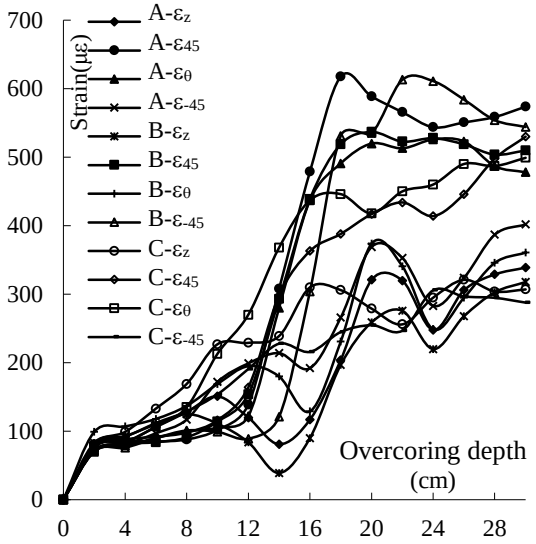

Figure 2. Typical curves of strain-overcoring distance (#7 point)

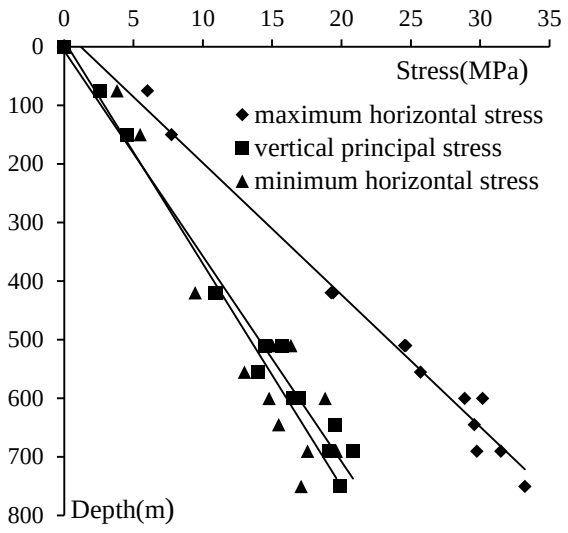

Figure 3. Linear regression of principal stresses with depth

The values of maximum horizontal principal stress ($\sigma_{h,\max}$), minimum horizontal principal stress ($\sigma_{h,\min}$) and vertical principal stress (σ_v) are all increased with depth and show approximately linear increasing regularity. Using linear regression method, the relations of magnitude of the stresses and the burring depth H are expressed as follows:

$$\sigma_{h,\max}=1.433+0.043H \quad (1)$$

$$\sigma_{h,\min}=1.304+0.024H \quad (2)$$

$$\sigma_v=0.07+0.028H \quad (3)$$

3. Rock permeability research

3.1 joint fissure distribution

Through joints survey in haulage way, stope and connection roadway, we collected 854 joints contain their strike, dip, trend, joint spacing, filling and seepage shown in table 2. Rose diagram of joints' strike and dip are shown in figure 4 and figure 5.

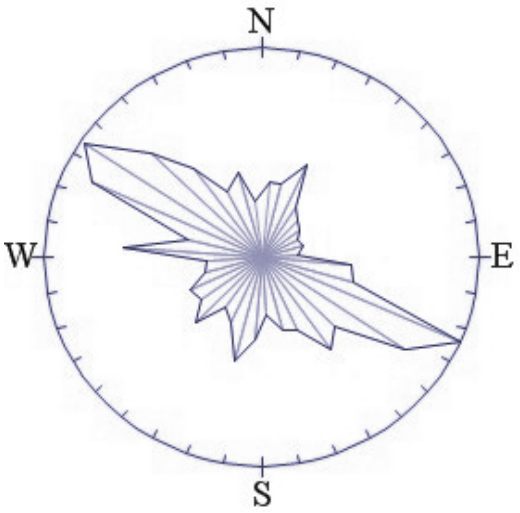

Figure 4. Rose diagram of joints' strike

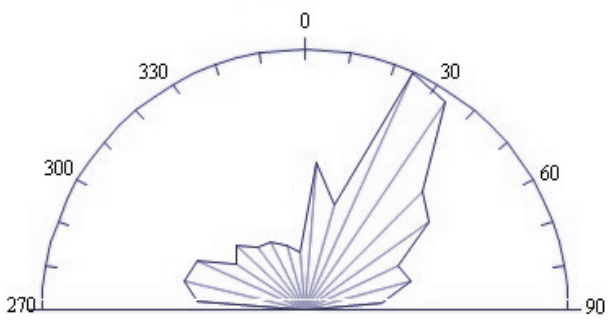

Figure 5. Rose diagram of joints' dip

Table 2. Joints distribution

strike /°	dip /°	percent /%	strike /°	dip /°	percent /%	strike /°	dip /°	percent /%
0-10	69	2.3	120-130	58	5.2	240-250	54	2.3
10-20	77	2.3	130-140	57	3.0	250-260	56	1.8
20-30	62	3.2	140-150	62	3.5	260-270	47	1.6
30-40	64	1.9	150-160	61	2.5	270-280	54	4.1
40-50	65	1.5	160-170	57	2.3	280-290	59	2.2
50-60	61	1.4	170-180	63	1.8	290-300	53	5.5
60-70	63	1.2	180-190	67	2.6	300-310	60	6.3
70-80	64	1.3	190-200	66	3.3	310-320	50	4.6
80-90	58	1.1	200-210	60	2.2	320-330	66	3.4
90-100	57	2.7	210-220	63	1.9	330-340	66	2.2
100-110	56	2.8	220-230	64	2.8	340-350	64	2.7
110-120	55	6.4	230-240	66	2.2	350-360	72	1.8

The rose diagrams show that there are 5 regnant strikes (20°～30° with average dip 62°, 110°～150°with average dip 57°, 190°～200°with average dip 66°, 270°～280°with average dip 54°, 290°～320° with average dip 55°) and 3 group regnant trend (5°, 20°～40° and 270°～280°, with dip between 40°~90°).

3.2 Rock permeability

(1) geometrical calculate

The geometrical calculate of permeability tensor was suggested by Snow[8]. For rock mass include M group joints, supposed every joints have no fillings, all the joints are extend unlimited and do not influence each other, defined geography north as X axis and east as Y axis, then the permeability K_i of the joint i can be expressed as:

$$K_i = \frac{\rho g b_i^3}{12\mu S_i}\begin{bmatrix} K_{xxi} & K_{xyi} & K_{xzi} \\ K_{yxi} & K_{yyi} & K_{yzi} \\ K_{zxi} & K_{zyi} & K_{zzi} \end{bmatrix} \quad (4)$$

Where, ρ is the water density with unit kg·m^{-3},

g is the gravitational acceleration with unit m·s^{-2},

b_i is the width of joint *i* with unit m,

μ is the water coefficient of dynamic viscosity with unit kg·(m^2·s)$^{-1}$,

$K_{xxi} = 1 - \sin^2\alpha_i \cos^2\beta_i$,

$K_{xyi} = K_{yxi} = -\sin^2\alpha_i \cos\beta_i \sin\beta_i$,

$K_{zxi} = K_{xzi} = -\sin\alpha_i \cos\alpha_i \cos\beta_i$,

$K_{yyi} = 1 - \sin^2\alpha_i \sin^2\beta_i$,

$K_{zzi} = \sin^2\alpha_i$,

α_i is the trend of joint *i*, $0 \le \alpha_i \le 360°$,

β_i is the dip of joint *i*, $0 \le \beta_i \le 90°$.

$$\begin{vmatrix} K_{xx} - A & K_{yx} & K_{zx} \\ K_{xy} & K_{yy} - A & K_{zy} \\ K_{xz} & K_{yz} & K_{zx} - A \end{vmatrix} = 0 \quad (5)$$

In equation (5), A_1、A_2 and A_3 are 3 principal value of permeability tensor, so the comprehensive permeability quotient can be calculated through the equation (6)[9-10]:

$$K = \sqrt[3]{A_1 A_2 A_3} \quad (6)$$

According to the above discussion, the comprehensive permeability quotient of in hanging side rock, ore body and heading side rock are calculated by the MATLAB in table 3.

Table 3. Permeability coefficients

rock areas	maximum value /m·s^{-1}	minimum value /m·s^{-1}	average value /m·s^{-1}
hanging side	9.1696×10^{-7}	4.3351×10^{-8}	7.3574×10^{-7}
heading side	1.7485×10^{-6}	8.5042×10^{-8}	7.9217×10^{-7}
ore body	2.0719×10^{-6}	1.2324×10^{-7}	9.4352×10^{-7}

(2) modification of permeability coefficient

In fact , joints in the rock mass are intersected and their extend range is limited which are different from the supposed conditions in geometrical calculate. So the permeability coefficients in table 3 should be modified through Monte-Carlo stochastic simulation[12,13], which is based on the occurrence and space of joints. Simulation results shows that the persistence ration of hanging side rock, ore body and heading side rock are 84.76%, 88.49% and 85.13%, shown in figure 6. Youtian Zhang[14] present $k = \eta k_0$ to modify the permeability coefficient k, and k_0 is the geometrical calculate value, η is the persistence ration. After modified, the average permeability coefficient values of hanging rock, ore body and heading rock are 6.2361×10^{-7}m·s^{-1}, 8.3492×10^{-7}m·s^{-1} and 6.7433×10^{-7}m·s^{-1}。

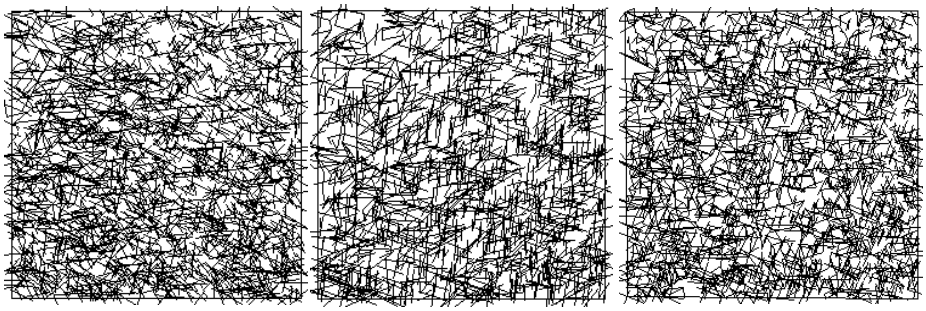

Figure 6. Persistence simulation by Monte-Carlo

Table 4. Physico-mechanical parameters

area	density /kg·m^3	bulk modulus /GPa	shear modulus /GPa	cohesive force /MPa	friction angle /°	strength exension /MPa	permeability coefficients /m·s^{-1}
hanging side	2706	3.37	2.8	11.4	31	4.37	6.2×10^{-7}

heading side	2635	5.48	3.45	42.8	37	5.98	6.7×10^{-7}
joints	2100	0.59	3.79	0.13	18	0.02	1.4×10^{-5}
ore body	2710	2.51	1.35	21.5	33	3.44	8.3×10^{-7}
filling mass	1600	0.9	0.75	0.8	20	0.08	2.5×10^{-6}

4. Simulation and fluid-mechanical coupling analysis

4.1 simulation model

Simulation model's elevation is between -430m and -1180m like figure 7. The size is 400m in X axis, 800m in Y axis and 800m in Z axis, and total 239508 zones and 256878 points. Simulate the mining process in -510m to-555m, which contain 8 adjacent stopes like figure 8 where stope is 10m wide and 30m long. The mining process is completed in 6 steps. The simulation physic-mechanical parameters are shown in Table 4.

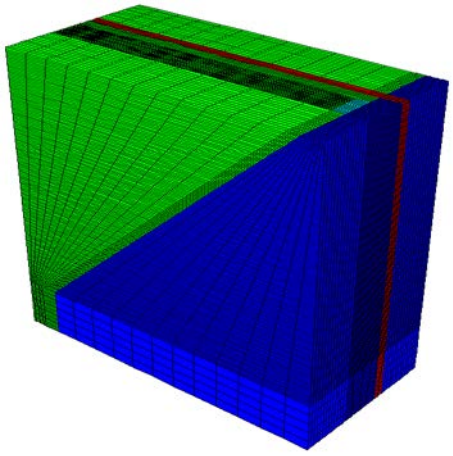

Figure 7. Simulation model

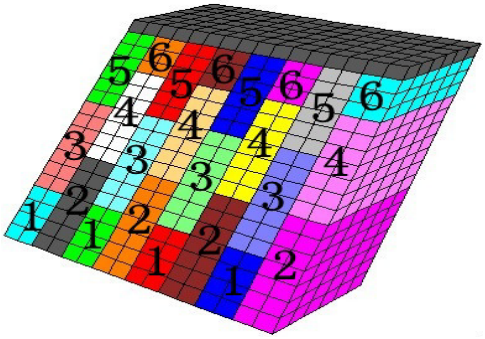

Figure 8. Mining steps

4.2 simulation results and analysis

(1) stope safety analysis

The maximum vertical displacement appeared in the center of the exploit area, and the extreme value of vertical displacement in the 6 steps are 7.753cm, 12.67cm, 17.471cm, 21.736cm, 22.625cm and 24.746cm. During the mining process, the vertical displacement increased gradually and present symmetrical characteristic as Figure 9. There are 2 groups: 1-4 stopes and 5-8 stopes, and a little displacement value zone between 4 and 5 stope.

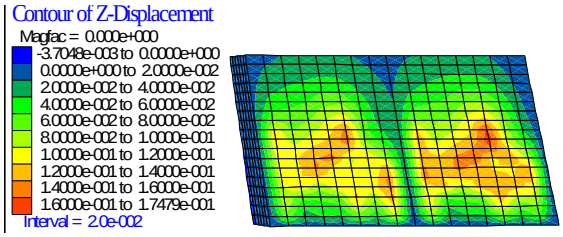

Figure 9. Vertical displacement of stope in 2nd mining step

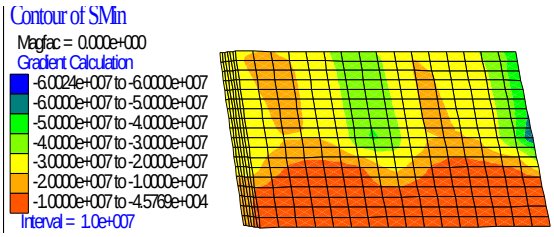

Figure 10. Maximum principal stress of stope in 2nd mining step

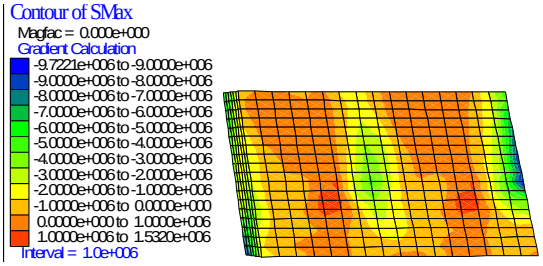

Figure 11. Minimum principal stress of stope in 2nd mining step

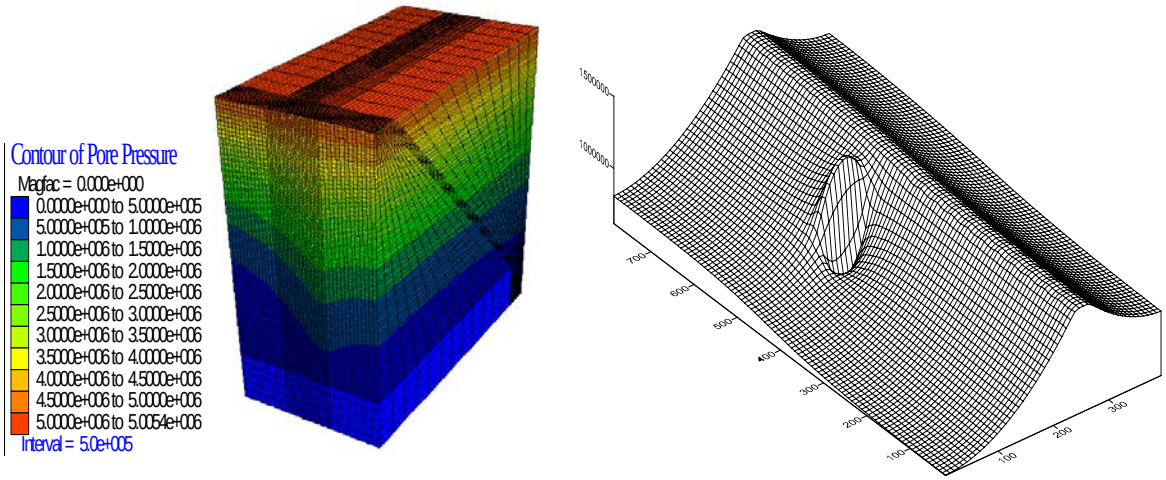

Figure 12. Seepage field

Figure 10 and figure 11 show the maximum and minimum principal stress distribution of the 2nd step. The maximum principal stresses of 6 steps are 50.073MPa, 60.024MPa, 52.398MPa, 67.959MPa, 52.603MPa and 43.048MPa, and this indicated the maximum principal stress in stopes 2, 4, 6, 8 are bigger than those in stopes 1, 3, 5, 7. The extreme value appears in stope 1 and there are stress concentration areas in stope 5. The minimum principal stress contours show that every mining step has tensile stress areas, and their extreme value are
2.656MPa、1.532MPa、1.484MPa、1.515MPa、1.362MPa、1.225MPa. The appearance of tensile stresses present regularly at stopes 2, 6 in first mining stage and at stopes 3, 7 in second stage.

5. Conclusions

Series of surveys and researches on water, joints and stress were completed in the coastal mine of Sanshandao Gold Mine: high density electrical prospecting was used to obtain the water distribution; permeability coefficients were achieved through geometric measurement and Monte-Carlo stochastic simulation.

Fluid-mechanical model was built to monitoring the deep mining process. The FLAC3D coupling model calculated the displacement and stress, found out the space-time distribution of displacement and stress fields. Based on the simulation, analyzed the seepage field and stress field distributions during the mining in different levels, as well as the ground pressure activity rules and seepage influence range, which are very important for the mining safety.

Acknowledge

This work was financially supported by the Fundamental Research Funds for the Central Universities (FRF-TP-14-038A1).

References

1. Cai M F. (2001) *Optimization of Mining Design and Control of Ground Pressure in Metal Mines-Theory and Practice*. Beijing: Science Press.
2. Wang C L, Wu A X, Liu X H, et al. (2010) Variation characteristics of capacity dimension Df with microseismicity in deep mining. *Journal of University of Science and Technology Beijing*, 32(11), p.p. 1379-1382.
3. Li X B, Liu Z X, Peng K et al. (2010) Theory and practice of rock mechanics related to exploitation of undersea metal mine. *Chinese Journal of Rock Mechanics and Engineering*, 29(10), p.p.1945-1953.
4. Z.X. Liu, W.G. Dang, X.Q. He (2012) Undersea safety mining of the large gold deposit in Xinli District of Sanshandao Gold

Mine. *International Journal of Minerals, Metallurgy and Materials*, 19(7), p.p.574-583.
5. Wang Q P, Xie N G, Shi X L. (2004) Fluid-soild dynamic coupling analysis of foundation soil during large deformation by dynamic consolidation. *Journal of University of Science and Technology Beijing*, 26(4), p.p.345-348.
6. Cai M F, Feng J Y, Wang J A. (2004) Three-dimensional hydraulic coupled stability of a high steep open pit slope. *Journal of University of Science and Technology Beijing*, 28(1), p.p. 6-11.
7. Qiao L, Ouyang Z H, Lai X P, et al. (2004) In-situ stress measurement and its result analysis in Sanshandao Gold Mine of China. *Journal of University of Science and Technology Beijing*, 26(6), p.p.569-571.
8. SNOW D T. (1969) Anisotropic permeability of fractured media. *Water Resources Research*, 5(6), p.p.1273-1289.
9. Chu Y Q. (1998) Determination methods of hydraulic parameters of rock mass(7). *Hydrogeology and Engineering Geology*, 25(2), p.p. 42-48.
10. Huang K Z, Xue M D, Lu M W. (2005) *Tensor Analysis*. Beijing: Tsinghua University Press.
11. Fang T, Chai J R, Hu H L et al. (2004) *Theory on Dynamics of Fluids in Fractured Medium*. Beijing: China Water & Power Press.
12. Fang T, Chai J R, Hu H L et al. (2007) Application of Monte Carlo method to simulating the fracture interconnectivity of rock mass. *Opencast Mining Technology*, No.1, p.p.7-9,13.
13. Du J C, Chen Z Y, Mi H L, et al. (2004) Determination of comprehensive shear strength for jointed rock massed in 3D condition using genetic algorithm and Monte-Carlo method. *Chinese Journal of Rock Mechanics and Engineering*, 23(13), p.p.2157-2163.
14. Zhang Y T. (2005) *Rock Hydraulics and Engineering*. Beijing: China Water & Power Press.